Electroluminescence from a n-ZnO nanorod/p-CuAlO2 heterojunction light-emitting diode

Qi, K. C.; Ling, Bo; Sun, Xiaowei; Zhao, Jun Liang; Tan, Swee Tiam; Dong, Zhili; Yang, Yi; Yu, Hongyu

2008

Ling, B., Sun, X., Zhao, J. L., Tan, S. T., Dong, Z. L., Yang, Y., et al. (2009). Electroluminescence from a n-ZnO nanorod/p-CuAlO2 heterojunction light-emitting diode. Physica E, 41(4), 635-639.

https://hdl.handle.net/10356/95679

https://doi.org/10.1016/j.physe.2008.10.017

Electroluminescence from a n-ZnO nanorod/p-$CuAlO_2$ heterojunction light-emitting diode

B. Ling [a], X.W. Sun [a,b,*], J.L. Zhao [a], S.T. Tan [b], Z.L. Dong [c], Y. Yang [a], H.Y. Yu [a], K.C. Qi [a]

[a] School of Electrical & Electronic Engineering, Nanyang Technological University, Nanyang Avenue, Singapore 639798, Singapore

[b] Institute of Microelectronics, 11 Science Park Road, Science Park II, Singapore 117685, Singapore

[c] School of Materials Science and Engineering, Nanyang Technological University, Nanyang Avenue, Singapore 639798, Singapore

** Corresponding author at: School of Electrical & Electronic Engineering, Nanyang Technological University, Nanyang Avenue, Singapore 639798, Singapore. Tel.: +65 67905369; fax: +65 67933318.*

E-mail address: exwsun@ntu.edu.sg (X.W. Sun).

Abstract

n-ZnO nanorod/p-$CuAlO_2$ heterojunction light-emitting diodes have been fabricated on p^+-Si substrates. The $CuAlO_2$ thin film was deposited by dc-magnetron sputtering while the ZnO nanorods (NRs) were fabricated using the vapor-phase transport method. The current–voltage characteristics of the devices showed good rectifying behavior with a high forward-to-reverse current ratio of around 120 at ± 7V. Strong ultraviolet electroluminescence centered at ~390 nm and a broad green-band emission were observed from the diode at room-temperature. The p-$CuAlO_2$ layer was found to facilitate hole injection from p^+-Si into n-ZnO while confining the electrons at ZnO/$CuAlO_2$ interface, thus effectively enhancing the recombination emission efficiency in ZnO NRs.

Keywords:
ZnO; Heterojunction; Light-emitting diode; UV emission

1. Introduction

ZnO has been recognized as one of the most promising photonic materials for ultraviolet (UV) light-emitting diodes (LEDs) with potential advantages over the III-nitride system because of its wide direct band gap (3.37 eV), large exciton binding energy (60 meV) and ease of wet etching [1,2]. Some interesting optical properties such as room-temperature (RT) UV lasing have been demonstrated in ZnO films and nanostructures [3–6]. Meanwhile, synthesis of one-dimensional single-crystalline ZnO nanostructures has

been of growing interest, owing to their improved optical properties compared to bulk materials, for example, thresholdless lasing [3,4] and promising application in nanoscale optoelectronic devices.

Based on a large number of studies performed on ZnO-based LEDs [7–18], the greatest challenge for realizing UV homostructure LEDs and even laser diodes lies in fabrication of low-resistivity, reliable and stable p-type ZnO. To avoid the difficulty of p-type doping, a number of heterojunctions consisting of n-type ZnO and other p-type semiconductors have been attempted to realize EL in the visible and UV regions [19–21]. Among various p-type counterparts, the delafossite $Cu^{I}M^{III}O_2$ class of materials, where M^{III} is a trivalent cation, have recently attracted great attention since they present p-type conductivity due to defect chemistry [22–25]. It is noteworthy here, although several groups have reported the fabrication of ZnO–$CuAlO_2$-based heterojunctions, they are generally investigated as photodiodes [26,27]. Although UV light emission from p-$SrCu_2O_2$/n-ZnO junctions was reported using pulsed laser deposition [28,29], there is no report on LEDs made of n-type ZnO nanorods (NRs) and p-type $CuAlO_2$.

In this paper, we shall report the fabrication and the characterization of stable UV-light-emitting heterojunctions composed of n-ZnO NR/p-$CuAlO_2$. The dense and aligned ZnO NRs fabricated by the vapor-phase transport (VPT) method provide high-quality channels for injection of electrons and natural optical confinement, while $CuAlO_2$ film fabricated by simple dc-magnetron sputtering facilitates the hole injection and confines electrons effectively.

2. Experiment

We used the p^+-Si (100) substrates in our experiments. Firstly, the p^+-Si wafers were ultrasonically cleaned in acetone and ethanol, followed by HF etching for 3min, and then rinsed in de-ionized water and dried by pure nitrogen gas. $CuAlO_2$ film was then fabricated on the p^+-Si wafer by dc-magnetron sputtering using a CuAl alloy target (Cu:Al = 70/30wt%, purity of 99.99%) in O_2/Ar (10/90vol%) gas under the working pressure of 10^{-3}Torr for 15min. The sputtering power was 100W and the thickness of the deposited $CuAlO_2$ was about 80 nm measured by a surface profiler (Tencor P-10). Thereafter, as-deposited $CuAlO_2$ films were annealed at 1050 ℃ in oxygen atmosphere for 30min under 600 Torr. A ZnO buffer layer (~70nm) was sputtered on the annealed $CuAlO_2$ film in order to obtain vertically aligned ZnO NRs by the VPT method.

The vertical ZnO NR arrays with diameters ranging from 300 to 500 nm and of length ~5 μm were fabricated on the ZnO buffer/$CuAlO_2$/p^+-Si substrates using the VPT method in a horizontal quartz tube furnace. ZnO (99.99%, Alfa Aesar) and graphite (99.99%,

Aldrich) powder were mixed (1:1 wt%) and used as the source material. The synthesis was carried out at 950 ℃ under a constant flow of 100 sccm Ar and 2 sccm O_2 under 1 Torr vacuum (maintained by a rotary pump). Detailed deposition procedure can be found elsewhere [30]. Before fabricating Au contact on the backside of the p^+-Si wafers, the substrates were etched by 2% HF solution to remove the native oxide. To prepare the Au cathode top contact on ZnO NRs, insulating hydrophobic poly(methyl methacrylate) (PMMA) as a supporting layer was spun-coated into the interspace between ZnO NRs. Several cycles of spin coating were carried out using 5 g/l PMMA in toluene onto ZnO NRs followed by drying in air to fill the interspace homogeneously. Then the O_2 plasma treatment was performed to expose ZnO NR top for Au contact deposition. Both Au electrodes on the front and the back of the device were prepared by the dc-magnetic sputtering. The top Au cathode (30 nm) was patterned into circular pads with diameter 1 mm using a shadow mask. For the purpose of optical and electrical characterizations, single layers of $CuAlO_2$ and ZnO NR were also deposited on quartz substrates and silicon substrates under the same condition, respectively. For comparison purpose, a control device n-ZnO NR/p^+-Si heterostructure LED without $CuAlO_2$ layer was also fabricated under the same condition so as to investigate the role of the $CuAlO_2$ layer.

The schematic diagram of the fabricated heterostructure LED is shown in Fig. 1. The surface morphology of the samples was investigated by an atomic force microscopy (AFM) (Digital Instruments NanoScope IIIa) and a JEOL JSM-5910LV scanning electron microscope (SEM). The crystal structure was characterized by the X-ray diffraction (XRD) using the Siemens D5005 X-ray diffractometer with Cu $K_{\alpha 1}$ radiation. Optical properties of $CuAlO_2$ film on glass substrates were measured by a UV–vis spectrometer HP 8453. The current–voltage (*I–V*) characteristics of the heterojunctions were investigated via a HP 4156A semiconductor parameter analyzer. The photoluminescence (PL) measurements were performed using a He–Cd laser (325 nm) as the excitation source. The EL measurements were performed using a photo-multiplier tube detector attached to a monochromator. All the characterizations were carried out at RT.

3. Results and discussion

Fig. 2 shows the XRD data of $CuAlO_2$ film before and after the annealing process with an AFM image of the annealed sample shown in the inset. The as-grown $CuAlO_2$ film shows no diffraction peaks, indicating the as-deposited film is amorphous. Whereas for the annealed film, distinct peaks are evident, indicating the film is crystallized after annealing. Besides the $CuAlO_2$ delafossite phase, some diffraction peaks from the $CuAl_2O_4$ phase can also be detected in the XRD pattern. The root mean square (RMS) of surface roughness of the annealed $CuAlO_2$ film (inset of Fig. 2) is only 3.7 nm, indicating

a smooth and homogeneous surface. Fig. 3 shows the optical transmission properties of annealed $CuAlO_2$ films on quartz. The annealed film showed high optical transmission above 90% in the visible region. From the transmittance data, we calculated the absorption coefficients (α) at the region of strong absorption using Manifacier model [31]. The fundamental absorption, which corresponds to electron excitation from valance band to the conduction band, can be used to determine the nature and value of the optical band gap. The relation between the absorption coefficient (α) and the incident photon energy ($h\nu$) can be written as [32,33]

$$(\alpha h\nu)^{1/n} = A(h\nu - E_g) \qquad (1)$$

where $h\nu$ is the photon energy, E_g is the optical band gap, A is a constant and n depends on the type of transition. For allowed indirect transition, n = 2; for allowed direct transition, n = 1/2. To determine the possible transitions, $(\alpha h\nu)^{1/n}$ (n = 1 and 1/2) vs. $h\nu$, are plotted as the insets of Fig. 3. By extrapolation (the insets of Fig. 3), $E_{g\text{-direct}}$ and $E_{g\text{-indirect}}$ are considered to be 4.2 and 2.4 eV, respectively. These values are slightly larger than those reported previously [27,34,35], which maybe due to the $CuAl_2O_4$ impurity phase that co-existed (Fig. 2).

Fig. 4(a) shows the XRD pattern of a wurtzite structure ZnO NRs with a dominant (0 0 0 2) growth orientation. Fig. 4(b) and the inset show the top view (10 ° tilted) of the as-grown ZnO NR array and the plasma-treated ZnO NRs with PMMA filling, respectively. We can see that the ZnO NRs grown on the ZnO buffer/$CuAlO_2$/p^+- Si substrates are well aligned with relatively uniform diameter (300–500 nm) and length (~5 μm). Fig. 4(c) shows a cross-section SEM image of ZnO NR arrays with PMMA filling. The arrows indicated the ZnO seed layer between the ZnO NR layer and the $CuAlO_2$ film.

The typical current–voltage (I–V) characteristics of n-ZnO NR/p-$CuAlO_2$/p^+-Si LED and n-ZnO NR/p^+-Si LED are shown in Fig. 5 and inset, respectively. Although both I–V curves show the typical rectifying characteristics of the diode, the device without the $CuAlO_2$ layer shows relatively high turn-on voltage (~5 V) and low break-down voltage (~7 V). However, the device with the $CuAlO_2$ layer shows a relatively low turn-on voltage of 4 V and a high break-down voltage above 40 V with a forward-to-reverse current ratio of ~120 at ± 7V.

Fig. 6(a) is the typical RT PL spectrum of ZnO NRs fabricated on the p^+-Si substrates under the same fabrication condition with a characteristic near-band-edge (NBE) emission of ZnO peak at ~378 nm (full-width at half-maximum of 10 nm) and a defect-related emission shoulder at ~492 nm. Under the forward bias with positive voltage

applied on the silicon substrate, both UV and deep-level emissions were detected at RT for the n-ZnO NR/p-$CuAlO_2$/p^+-Si LED and the n-ZnO NR/p^+-Si LED. Fig. 6(b) illustrates the RT EL spectra of n-ZnO NR/p-$CuAlO_2$/p^+-Si LED at various forward injection currents. The spectrum is dominated by a predominant UV emission peak centered at ~390 nm corresponding to NBE emission of ZnO. The weak broadband centered at 500–550 nm should be related to the transition from the defect energy level to the valence band [36]. The green light is clearly observed from the LED by naked eyes at RT as shown in the right inset of Fig. 6(b). The EL intensity of the broad green band peak grows linearly with the current density while the intensity of UV peaks rise abruptly when the injection current increases from 40 to 60 mA. Fig. 6(c) shows the EL spectrum of our control device without the $CuAlO_2$ layer (n-ZnO NR/p^+-Si). The intensity ratio of the UV emission to defect level emission is much weaker compared with that of n-ZnO NR/p-$CuAlO_2$/p^+-Si LED [Fig. 6(b)], suggesting that the $CuAlO_2$ film is essential in improving the performance of ZnO/Si UV LEDs. The EL photo of the n-ZnO NR/p^+-Si LED is shown as inset of Figs. 6(c). The spotty emission photos [Fig. 6(a) and (b)] are possibly due to the optical confinement of ZnO NRs. The difference in brightness on the edge and in the center of the top contact is simply due to Au thickness difference. It is worth mentioning that we tested our n-ZnO NR/p-$CuAlO_2$/p^+-Si LEDs again after keeping them under ambient air at RT for 6 months; the green light emission still can be seen by the naked eyes from these LEDs without encapsulation.

In order to illustrate the mechanism of light generation in our LED, the expected energy band diagram of n-ZnO NR/p-$CuAlO_2$/ p^+-Si LED at zero and forward bias were shown in Figs. 7(a) and (b), respectively. To simplify the analysis, here we neglect the effects of dipole, interfacial state and native silicon oxide layer between the $CuAlO_2$ film and silicon substrate. Under forward bias, holes in the p^+-Si substrates firstly, flow into the valence band of $CuAlO_2$ and then flow together with the holes in the $CuAlO_2$ layer into the valence band of the ZnO seed layer while electrons are injected into this seed layer from the ZnO NR layer via the Au electrode at an appropriate negative voltage. Since the large direct band gap of $CuAlO_2$ as calculated before causes the large band gap offset between the conduction band of $CuAlO_2$ and ZnO, the electrons were well confined in the ZnO layer, thus enhancing the near band edge emission (NBE) of ZnO [Fig. 6(b)] by favoring the recombination of electrons and holes and also resulting in the much higher break-down voltage of the device compared with the device without the $CuAlO_2$ layer [Fig. 6(c)]. Here the $CuAlO_2$ film has two functions, (1) to improve the hole injection to the ZnO layer and (2) to work as an energy barrier layer to confine the electrons in the ZnO layer, thus resulting in efficient recombination. A possible EL emission path in our device is proposed based on the aforementioned analysis, as shown in Fig. 7(c). The EL emission comes from the ZnO seeding layer which forms at the interface between ZnO NR and $CuAlO_2$, and is then funneled into ZnO NRs. The UV light traveling in ZnO NR

can be reabsorbed by ZnO and re-emitted (polariton) [37,38]. This is reflected in the redshift (10 nm) of UV EL peak compared with the PL of ZnO NRs (Fig. 6). It is worth mentioning that ZnO NRs not only provide high-quality channels for the electrons injection but also natural optical confinement here. Electron transport in the nanorods should be better than in a continuous ZnO film due to its good single crystallinity and high mobility. Moreover, the contact size in our nanostructure-based device is much smaller than that of a film-based device, so the carrier injection rate significantly increases in the Schottky diodes [39–41]. In addition, the vertically aligned ZnO nanorods can act as waveguides and a high lateral confinement of the light emitted from the junction [42,43].

4. Conclusion

In conclusion, we have demonstrated UV-emitting LEDs based on n-ZnO-NR/p-$CuAlO_2$ as a heterostructure synthesized by the VPT and the dc-magnetron sputtering techniques. The n-ZnO NR/p-$CuAlO_2$/p^+-Si LEDs emit a strong UV light (~390 nm) at RT and showing good rectifying characteristics with a low leakage current under reversed bias. Compared to n-ZnO NR/p^+-Si LEDs, the insertion of the $CuAlO_2$ layer was found to facilitate hole injection, while confining electrons under forward bias, thus enhancing the NBE emission of ZnO. The EL should be originally generated in the ZnO seed layer and enhanced in upper ZnO NRs due to photoexcited excitons present, which needs further investigation. Further experiment is to get more high-quality seed layer to remove (decrease) the electroluminescence from defects.

References

[1] D.C. Look, Mater. Sci. Eng. B 80 (2001) 383.
[2] X.W. Sun, H.S. Kwok, J. Appl. Phys. 86 (1999) 408.
[3] D.M. Bagnall, Y.F. Chen, Z. Zhu, T. Yao, S. Koyama, M.Y. Shen, T. Goto, Appl. Phys. Lett. 70 (1997) 2230.
[4] Z.K. Tang, G.K.L. Wong, P. Yu, M. Kawasaki, A. Ohtomo, H. Koinuma, Y. Segawa, Appl. Phys. Lett. 72 (1998) 3270.
[5] H.Q. Yan, R.R. He, J. Johnson, M. Law, R.J. Saykally, P.D. Yang, J. Am. Chem. Soc. 125 (2003) 4728.
[6] X.W. Sun, J.Z. Huang, J.X. Wang, Z. Xu, Nano Lett. 8 (2008) 1219.
[7] A.L. Burin, M.A. Ratner, H. Cao, S.H. Chang, Phys. Rev. Lett. 88 (2002) 093904.
[8] C. Bouvy, E. Chelnokov, R. Zhao, W. Marine, R. Sporken, B.L. Su, Nanotechnology 19 (2008) 105710.
[9] T. Aoki, Y. Hatanaka, D.C. Look, Appl. Phys. Lett. 76 (2000) 3257.
[10] Y.R. Ryu, T.S. Lee, J.H. Leem, H.W. White, Appl. Phys. Lett. 83 (2003) 4032.
[11] Y.I. Alivov, E.V. Kalinina, A.E. Cherenkov, D.C. Look, B.M. Ataev, A.K. Omaev, M.V. Chukichev, D.M. Bagnall, Appl. Phys. Lett. 83 (2003) 4719.
[12] A. Tsukazaki, A. Ohtomo, T. Onuma, M. Ohtani, T. Makino, M. Sumiya, K. Ohtani, S.F. Chichibu, S. Fuke, Y. Segawa, H. Ohno, H. Koinuma, M. Kawasaki, Nat. Mater. 4 (2005) 42.
[13] Y.R. Ryu, T.S. Lee, J.A. Lubguban, H.W. White, B.J. Kim, Y.S. Park, C.J. Youn, Appl. Phys. Lett. 88 (2006) 241108.
[14] J.H. Lim, C.K. Kang, K.K. Kim, I.K. Park, D.K. Hwang, S.J. Park, Adv. Mater. 18 (2006) 2720.
[15] J.L. Zhao, X.W. Sun, S.T. Tan, G.Q. Lo, D.L. Kwong, Z.H. Cen, Appl. Phys. Lett. 91 (2007) 263501.
[16] X.W. Sun, J.L. Zhao, S.T. Tan, L.H. Tan, C.H. Tung, G.Q. Lo, D.L. Kwong, Y.W. Zhang, X.M. Li, K.L. Teo, Appl. Phys. Lett. 92 (2008) 111113.
[17] R. Könenkamp, R.C. Word, C. Schlegel, Appl. Phys. Lett. 85 (2004) 6004.
[18] R. Könenkamp, R.C. Word, M. Godinez, Nano Lett. 5 (2005) 2005.
[19] H. Ohta, M. Orita, M. Hirano, H. Hosono, J. Appl. Phys. 89 (2001) 5720.
[20] Y.I. Alivov, J.E. Van Nostrand, D.C. Look, M.V. Chukichev, B.M. Ataev, Appl. Phys. Lett. 83 (2003) 2943.
[21] C. Yuen, S.F. Yu, S.P. Lau, Rusli, T.P. Chen, Appl. Phys. Lett. 86 (2005) 241111.
[22] H. Kawazoe, M. Yasukawa, H. Hyodo, M. Kurita, H. Yanagi, H. Hosono, Nature 389 (1997) 939.
[23] A.N. Banerjee, K.K. Chattopadhyay, J. Appl. Phys. 97 (2005) 084308.
[24] K. Ueda, S. Inoue, S. Hirose, H. Kawazoe, H. Hosono, Appl. Phys. Lett. 77 (2000) 2701.

[25] H. Hiramatsu, K. Ueda, H. Ohta, M. Orita, M. Hirano, H. Hosono, Thin Solid Films 411 (2002) 125.
[26] K. Yonooka, H. Bando, Y. Aiura, Thin Solid Films 445 (2003) 327.
[27] A.N. Banerjee, S. Nandy, C.K. Ghosh, K.K. Chattopadhyay, Thin Solid Films 515 (2007) 7324.
[28] H. Ohta, K. Kawamura, M. Orita, M. Hirano, N. Sarukura, H. Hosono, Appl. Phys. Lett. 77 (2000) 475.
[29] H. Hosono, H. Ohta, K. Hayashi, M. Orita, M. Hirano, J. Cryst. Growth 237–239 (2002) 496.
[30] Y. Yang, X.W. Sun, B.K. Tay, J.X. Wang, Z.L. Dong, H.M. Fan, Adv. Mater. 19 (2007) 1839.
[31] J.C. Manifacier, J. Gasiot, J.P. Fillard, J. Phys. E 9 (1976) 1002.
[32] J.I. Pankove, Optical Processes in Semiconductors, Prentice-Hall Inc., New Jersey, 1971, p. 34.
[33] S.T. Tan, B.J. Chen, X.W. Sun, W.J. Fan, H.S. Kwok, X.H. Zhang, S.J. Chua, J. Appl. Phys. 98 (2005) 013505.
[34] H. Yanagi, S. Inoue, K. Ueda, H. kawazoe, H. Hosono, N. Hamada, J. Appl. Phys. 88 (2000) 4159.
[35] J. Robertson, P.W. Peacock, M.D. Towler, R. Needs, Thin Solid Films 411 (2002) 96.
[36] N.O. Korsunska, L.V. Borkovska, B.M. Bulakh, L.Yu. Khomenkova, V.I. Kushnirenko, I.V. Markevich, J. Lumin. 102–103 (2003) 733.
[37] G. Malpuech, M.M. Glazov, I.A. Shelykh, P. Bigenwald, K.V. Kavokin, Appl. Phys. Lett. 88 (2006) 111118.
[38] L.K. Vugt, S. Rühle, P. Ravindran, H.C. Gerritsen, L. Kuipers, D. Vanmaekelbergh, Phys. Rev. Lett. 97 (2006) 147401.
[39] W.I. Park, G. Yi, Adv. Mater. 16 (2004) 87.
[40] G.D.J. Smit, S. Rogge, T.M. Klapwijk, Appl. Phys. Lett. 81 (2002) 3852.
[41] W.I. Park, G. Yi, J.W. Kim, S.M. Park, Appl. Phys. Lett. 82 (2003) 4358.
[42] R. Hauschild, H. Kalt, Appl. Phys. Lett. 89 (2006) 123107.
[43] M. Matsuu, S. Shimada, K. Masuya, S. Hirano, M. Kuwabara, Adv. Mater. 18 (2006) 1617.

List of Figures

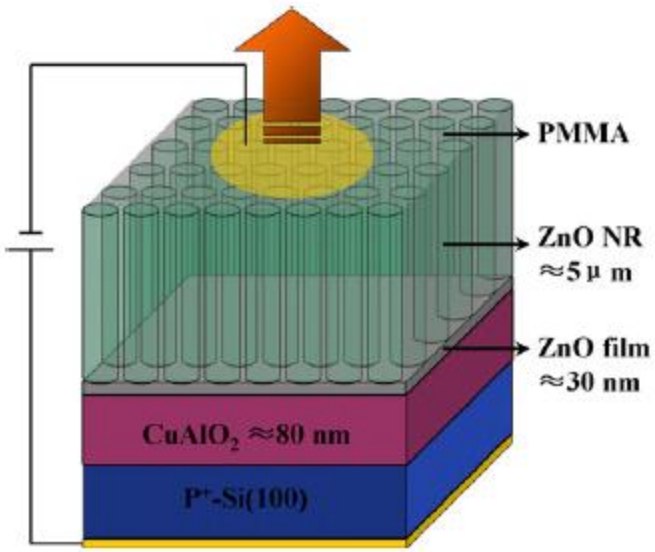

Figure 1

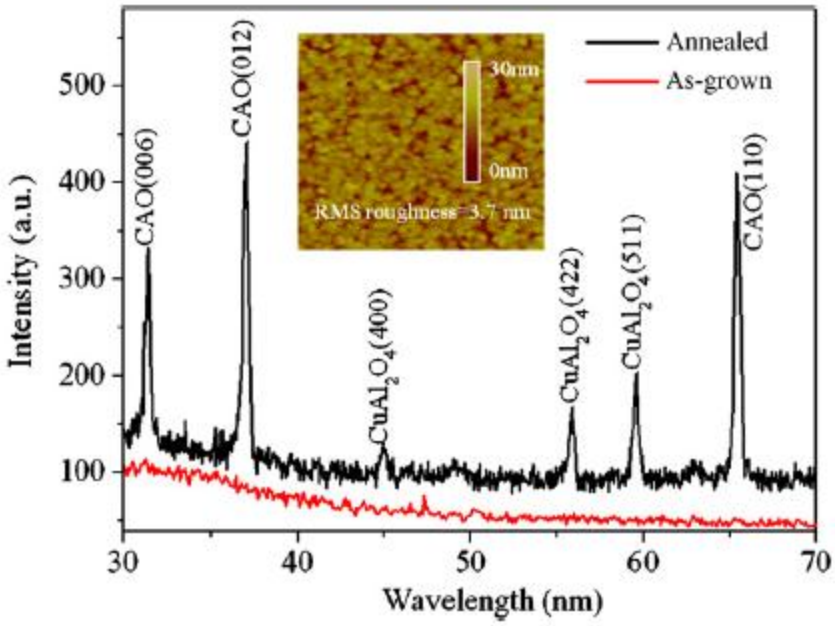
Annealed
As-grown
30nm
0nm
RMS roughness=3.7 nm
CAO(006)
CAO(012)
CuAl2O4(400)
CuAl2O4(422)
CuAl2O4(511)
CAO(110)
Intensity (a.u.)
Wavelength (nm)
100
200
300
400
500
30
40
50
60
70

Figure 2

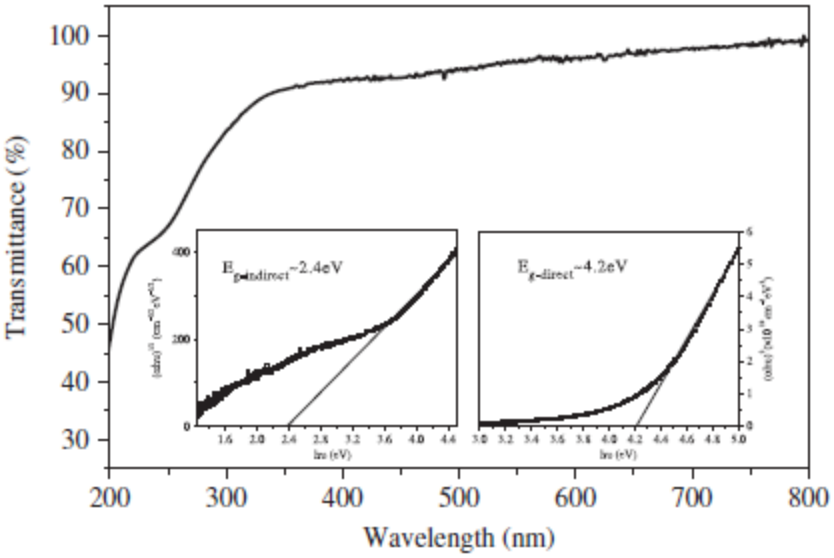
Transmittance (%)
Wavelength (nm)
E_g-indirect~2.4eV
E_g-direct~4.2eV
hν (eV)
hν (eV)

Figure 3

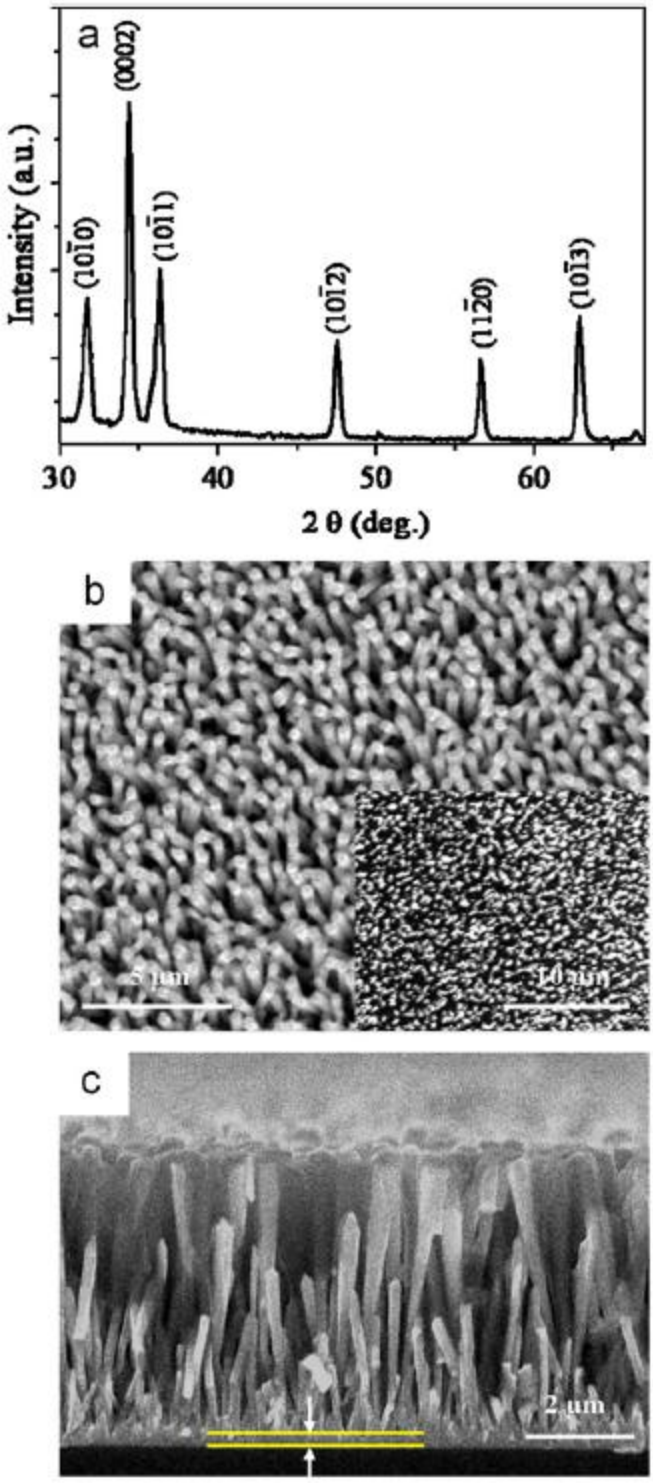
a
(0002)
(10$\bar{1}$0)
(10$\bar{1}$1)
(10$\bar{1}$2)
(11$\bar{2}$0)
(10$\bar{1}$3)
Intensity (a.u.)
30
40
50
60
2 θ (deg.)
b
5 μm
10 μm
c
2 μm

Figure 4

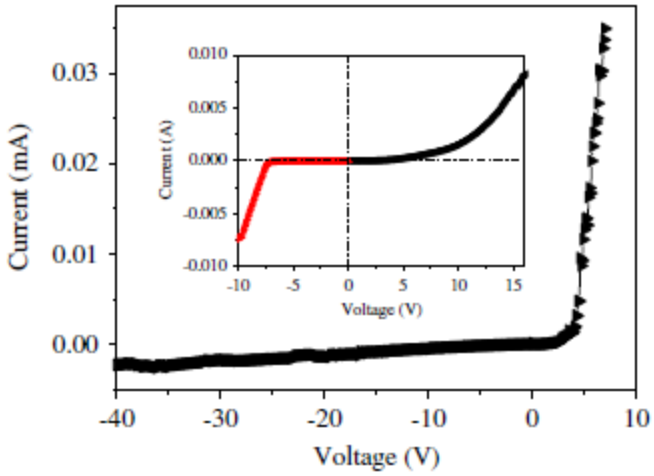
Current (mA)
0.03
0.02
0.01
0.00
-40
-30
-20
-10
0
10
Voltage (V)
Current (A)
0.010
0.005
0.000
-0.005
-0.010
-10
-5
0
5
10
15
Voltage (V)

Figure 5

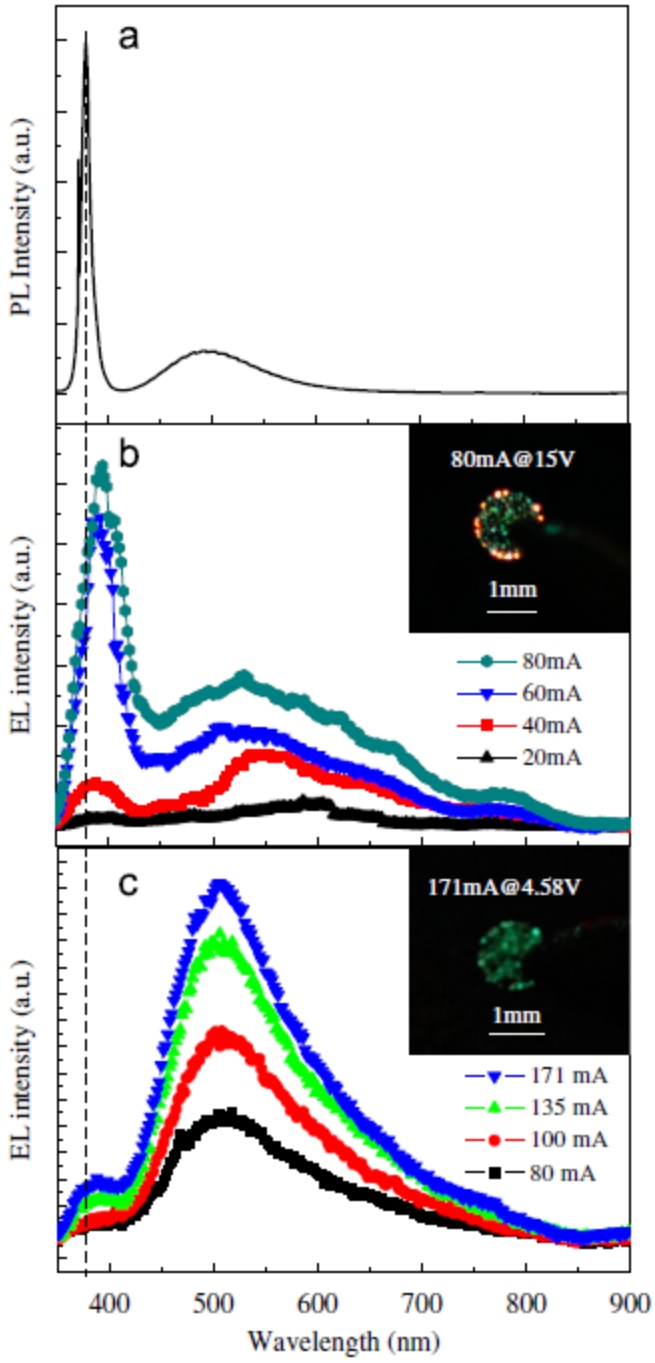
a
PL Intensity (a.u.)
b
EL intensity (a.u.)
80mA@15V
1mm
80mA
60mA
40mA
20mA
c
EL intensity (a.u.)
171mA@4.58V
1mm
171 mA
135 mA
100 mA
80 mA
400
500
600
700
800
900
Wavelength (nm)

Figure 6

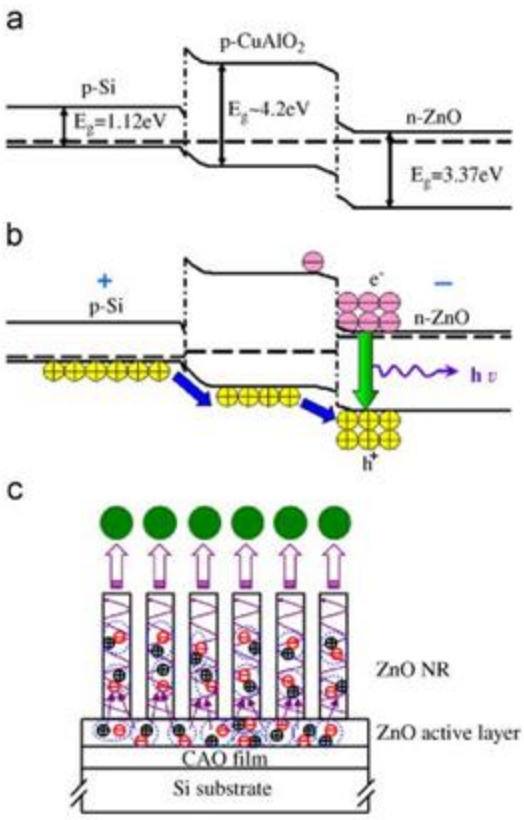
a
p-CuAlO2
p-Si
Eg=1.12eV
Eg~4.2eV
n-ZnO
Eg=3.37eV
b
+
p-Si
e-
−
n-ZnO
h υ
h+
c
ZnO NR
ZnO active layer
CAO film
Si substrate

Figure 7